



Analysis of the refugees' drowning events: the earthquakes' statistics analogy

Ashod Khederlarian¹, Martin Grant², Monika Halkort³, Sara Najem^{1,a}

¹ Physics Department, American University of Beirut, Beirut 1107 2020, Lebanon

² Physics Department, McGill University, Rutherford Building, 3600 Rue University, Montréal, Québec H3A 2T8, Canada

³ Department of Communication Arts, Lebanese American University, Chouran Beirut 1102 2801, Lebanon

Received: 1 March 2021 / Accepted: 26 May 2021

© The Author(s), under exclusive licence to Società Italiana di Fisica and Springer-Verlag GmbH Germany, part of Springer Nature 2021

Abstract In this paper, we explore the analogy between the refugees' drownings in the sea and the earthquakes' occurrences and focus on the aspect that characterizes the statistics of their spatial and temporal successions. The latter is shown to parallel the spatial distribution of consecutive drowning events with the difference that the former exhibits short-range behavior below $\kappa = 4$ km and it is characterized by scale-free statistics, as well as finite size scaling beyond $\kappa = 4$ km, with a critical exponent $\delta \approx 0.5$, falling within the range of the earthquakes' $\delta = 0.6 \pm 0.2$, while the distribution of events' rates exhibits no similarity with that of the earthquakes. Finally, the events' velocity distribution is also recovered. κ is suspected to be related to the range of mobile network's coverage and thus effectively represents a cutoff in the ability of picking up signals on drownings in the sea.

1 Introduction

The study of spatiotemporally varying phenomena spans a wide spectrum of disciplines and systems whose objective is to reveal patterns of the underlying, often not too well understood, dynamical processes. These include just to list a few: astrophysical questions concerned with accretion [1], geological applications specifically earthquakes and landslides [2–5], the study of epidemics, like Ebola and Malaria [6, 7], natural hazards such as forest fires [8], problems in economics and finance [9], various systems in condensed matter and material science namely superconductors [10], all the way to neural dynamics and the complexity of brain activity and heart rate [11–15]. These spatiotemporal phenomena are examined not through the individual isolated space-time events but rather through the latter's interdependence and correlation. Within this framework, systems exhibiting power-law behaviors are said to be poised at criticality [2, 16] and the question of whether they can be explained as self-organized critical systems had been a matter of debate. Further, a more disputable question is whether or not the conclusion drawn for these systems can be extended to human behavior, be it at the cognitive or social levels [17–20].

^a e-mail: sn62@aub.edu.lb (corresponding author)

These borrowed notions from statistical physics are increasingly finding their way to the analysis of high-volume crime patterns, the characterization of human mobility, and in refugee migration [3–7, 21–24]. The understanding of the statistics of such tragic (in some cases catastrophic) events and often the ability to predict them is pivotal in crises management and prevention. Of particular interest is the drowning of refugees crossing the Mediterranean, which is considered as the deadliest migration route in the world, with over 14,500 deaths reported between 2014 and 2017 [25]. Further, as analogies between social behavior with natural catastrophes are explored, like the case of transgressive contention and its equivalence to waves of wildfires [26], and taking the metaphor of drownings incidents as ground-shaking events seriously [27, 28], we set to explore the similarity between the refugee drownings and earthquakes. We suspect that once human-trafficking routes are defined they constitute fault lines along which the drownings are likely to happen.

The spatiotemporal analysis of these events revealed that the probability distribution of jumps, defined as the distance between consequent events, is very similar to the one in [3] for intermediate and long-ranged distances; however, it is characterized by a short-ranged repulsive dynamics (without scaling). Also, the velocity of propagation of events followed a scaling law, with the scaling function interestingly behaving like the unscaled distribution of [3], with an initial plateau, followed by an exponential decrease, ending with a rather sharp cutoff. We finally wonder whether the patterns this analysis reveals are tied to the mobile coverage, which limit the drownings to “detectable zones” compared to others, where “invisible drownings” may occur and remain undetected.

2 Methodology

Watch the Med’s website reports the drowning events [29], which we scraped and transformed into a dataset that includes information about their dates, reporting times, locations, latitudes, longitudes, and events’ descriptions. The data spanning the Mediterranean sea were gridded by doing a Mercator Projection for four different grid sizes $L = [S/3, S/6, S/9, S/12]$, with $S = 4290\text{km}$ being the diagonal of the full area where there is just one cell. Within each grid cell, the time intervals (Δt_i) and great-circle distances (Δr_i) of successive events were calculated [30]. Then, the probability density of the spatial separation $P(L, \Delta r)$ was obtained by binning the interval $[\Delta r_{\min}; \Delta r_{\max}]$, counting the number of Δr ’s within each bin, and dividing by the bin width. Of course, because of the multiple length (and time) scales involved in the data, consecutive bin widths were made to increase exponentially so that they look equally spaced on a logarithmic scale. For every grid size L , a single function $P(L, \Delta r)$ is computed, which is the average of the probability densities of all grid-cells having size L . For statistical reasons, grid-cell which had less than six events weren’t included in the analysis. Furthermore, separations less than 250m were ignored.

As for the temporal analysis of the data, the exact same procedure was followed; however, now with each grid size L there is an associated mean rate R , defined as the total number of events in a given region divided by the total time interval over which these events span. It was calculated by applying this definition within a single cell and averaging over all cells. The values obtained were $[0.028, 0.022, 0.011, 0.012](/hr)$ for the different grid sizes mentioned above, respectively. The computation of the velocity distribution, defined as $v = \frac{\Delta x}{\Delta t}$, was also carried out following the same methodology described above.

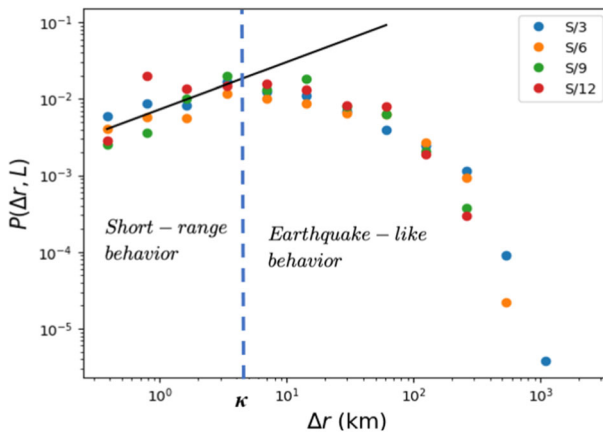


Fig. 1 The figure shows the non-scaled $P(L, \Delta r)$ along with the line fitting the short-range behavior whose slope is 0.62 and a corresponding standard deviation of 0.14

3 Results

3.1 Characterization of $P(L, \Delta r)$

We find that $P(L, \Delta r)$ is composed of three regimes corresponding to short, intermediate, and long-range behaviors as shown in Fig. 1. The first corresponds to an increase in $P(L, \Delta r)$, followed by a decrease and a sharp tail. In the second and third regimes, the distribution is reminiscent of that of consecutive earthquakes [3]. The latter was shown to follow scale-free statistics, as well as finite-size-scaling, with exponents $\delta = 0.6$, and $\alpha = 1$ which is given in Eq. 1, while δ is defined to be the power controlling the decay of $f(x)$ with respect to its argument given by $f(x) \approx x^{-\delta}$. All these can be cast into:

$$P(L, \Delta r) = \frac{f(\Delta r/L^\alpha)}{L^\alpha} \tag{1}$$

For the drownings, we found $\alpha \approx 1$ and $f(x)$ decreases as $x^{-\delta}$ with $\delta \approx 0.49$ for $x < 0.1$ and decays quickly for $x > 0.1$ when compared to the exponents of the earthquakes' rescaled distribution as shown in Fig. 2. It is worth noting that $f(x)$ is a Lévy-flight as it is controlled by a fractional power beyond a critical threshold which is in line with the literature on individual motion and swarm dynamics [31]

3.2 Temporal distribution

The inter-event time distribution $P(R, \Delta t)$ revealed a similar scaling law given in Eq. 2:

$$P(R, \Delta t) = \frac{g(\Delta t R^\beta)}{R^{-\beta}} \tag{2}$$

The un-scaled plot of the probability density of inter-event times is shown in Fig. 3. It is clear that this distributions spans many orders of magnitudes, more so than the jump distribution. Disregarding the points below 3×10^4 s, as they only make up less than 4% of the data and focusing on the remaining 96%, we could clearly recover the scaling given in Eq. 2, with

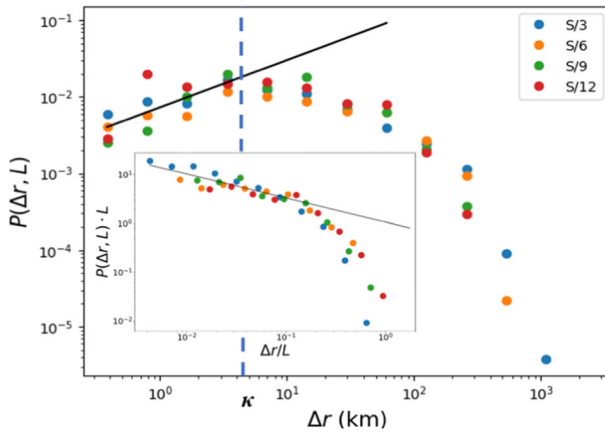


Fig. 2 The un-scaled jump distribution is shown along with the inset showing the scaled distribution for intermediate and large values of Δr . beyond $\kappa = 4\text{km}$. The slope of line is given by -0.49 with standard deviation 0.07

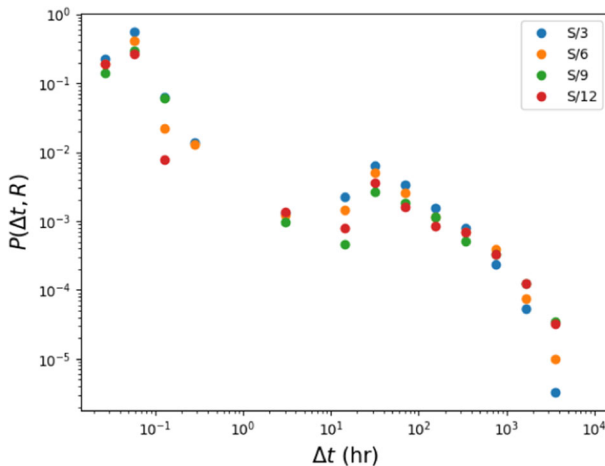


Fig. 3 The figure shows the un-scaled inter-event time distribution

$\beta \approx 1$ and $g(x)$ flat up to $x = 1$ with a transition to an exponentially decreasing regime $x^{-\gamma}$ with $\gamma \approx 0.96$ and a tail after $x \approx 30$ as shown in Fig. 4. Such a scaling with R is similar to the one found for earthquakes in [4], albeit with a different scaling function. In order to better assess the quality of the collapse for this noisy data, we follow its cumulative probability distribution given by $P(y) = \int_0^y P(x, L) dx$. Using Eq. 2, we can write $P(y)$ as in Eq. 3:

$$P(y) = \int_0^y \frac{f(\Delta t R^\beta)}{R^{-\beta}} d(\Delta t) = \int_0^y f(\Delta t R^\beta) d(\Delta t R^\beta) \tag{3}$$

which clearly shows that plotting $P(y)$ versus $\Delta t R^\beta$ leads to a data of $f(\Delta t R^\beta)$ as shown in Fig. 5.

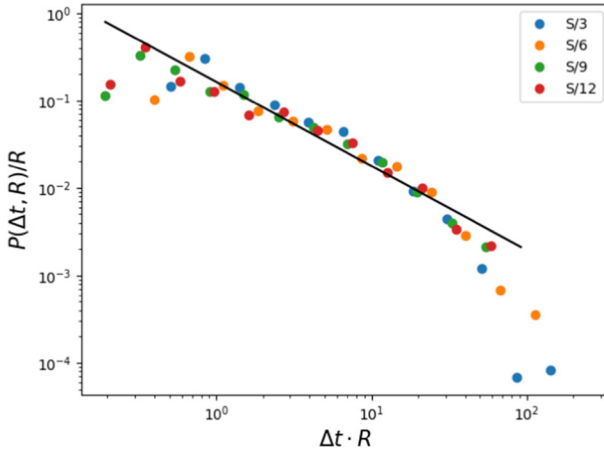


Fig. 4 The figure shows the scaled inter-event time distribution. The line has a slope of -0.96 with standard deviation 0.05

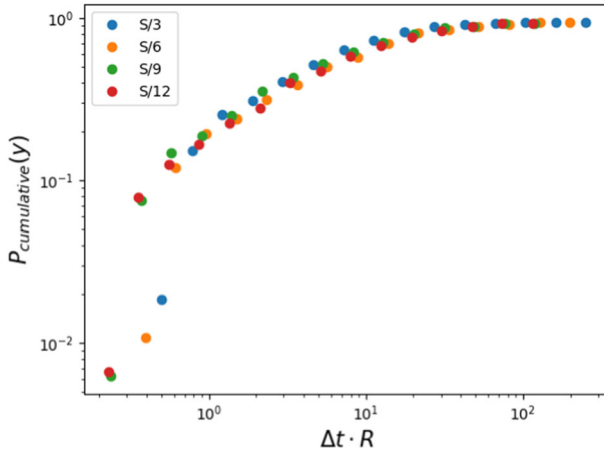


Fig. 5 The cumulative probability distribution of inter-event times is shown in

3.3 Velocity distribution

Finally, we find that the velocity distribution is also described by a similar finite-size-scaling given by Eq. 4

$$P(L, \Delta v) = \frac{h(\Delta v / (LR)^\eta)}{(LR)^\eta} \tag{4}$$

where $\Delta v = \frac{\Delta r}{\Delta t}$, $\eta \approx 1$, and $h(x)$ is flat up to $x \approx 3 \times 10^{-3}$, decays as $x^{-\zeta}$ with $\zeta \approx 1$ within the range $[3 \times 10^{-3}, 3 \times 10^{-1}]$, and ends with a sharp cutoff as shown in Fig. 6.

4 Discussion

From the results shown in Figs. 1 and 2, we can conclude that there is a short-range behavior which corresponds to $\Delta r < \kappa$ where the probability of an incidence occurrence increases with distance. Beyond that it decreases with no characteristic length scale obeying the finite-size-scaling ansatz given in Eq. 1. Moreover, for $\Delta r < \kappa$ we note that these events are clustered around the shores as shown in Fig. 7 which might be resulting from the mobile coverage zones.

More precisely, the incidents are more likely to get detected near the shores followed by a drop in the probability of detection beyond $\kappa = 4$ km. Therefore, this might have far reaching implications; that is if the radars’ coverage and mobile networks of both the guards and the refugees are limited to buffer zones around the shores then the signals for rescue would only be picked up within radii of 4 km from the clusters’ epicenters and most call for rescue attempts are not even detected. This leads us to conclude that the statistics we are observing result from the limitation of the surveillance in the sea and extension of coverage beyond its current state might increase the chances of rescue. The potential mismatch between the actual detected and the “potential undetected events” is illustrated in Fig. 8, where the cutoff of the increasing line is set by the normalization condition.

Further, and since L represents the diagonal of the grid-cell rectangle, it is clear that the cutoff in the inset of Fig. 2 is due to the fact that the jumps cannot be greater than the diagonal

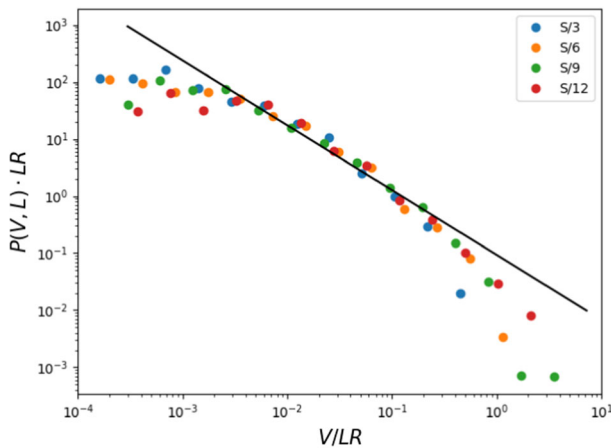


Fig. 6 The velocity-scaled distribution fitted line has slope -1.1

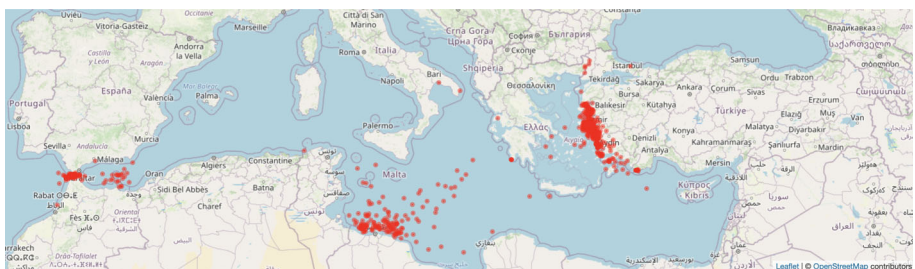


Fig. 7 The figure shows the map of the drowning events’ locations exhibiting clustering around the shores

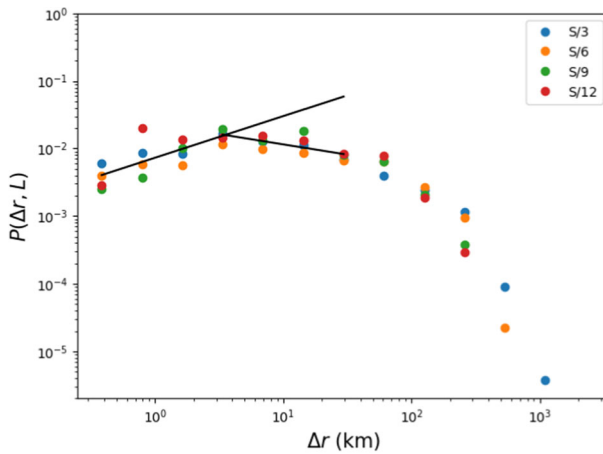


Fig. 8 The figure shows the potential mismatch in event detection.

of the rectangle, and so the probability has to decay to 0 at $\Delta r/L = 1$, which also applies in the earthquakes' case, with a cutoff $\Delta r/L = 1/2$, compared to that of the drownings at $\Delta r/L = 0.1$. As for the inter-event time distribution shown in Fig. 3, we also note that the short inter-event time had to be excluded. However, if the curve of Fig. 4 was to be interpolated to short inter-event times it would reveal a higher probability of drownings for small Δt . These short-inter-event times are also missed potentially because of the loss of network coverage in the sea or the insufficiency of the first responders. This furthers hints that more incidents are occurring at times-scale which cannot be picked up for the above laid out argument.

Finally, in trying to understand the limits of the velocity distribution, we note that small V corresponds to small r and large t , since $\Delta V = \Delta r/\Delta t$: these correspond to $\Delta r \approx 10^{-2}L$ and $\Delta t \approx 10^2/R$, which give $\Delta V_{small} \approx 10^{-4}(LR)$. The same reasoning gives $\Delta V_{large} \approx 10(LR)$. These limits suggest that V should not scale with L solely, but rather with RL , as shown in Fig. 6.

Equivalently, the speed at which the events occur depends on the extent of spatial and temporal coverage and thus the ability to pick up rescue signals from the sea. Since this is limited by κ , we will be at the false of impression of a process happening at a slower rate that it really is and thus the gravity of the situation gets toned down leading us to conclude that actual value of δ should be less than 0.49 ± 0.07 .

5 Conclusion

In this paper, we have explored the spatiotemporal time series of drowning events of refugees in the sea. This has revealed the extent to which signals can be received relying on the scale-free nature of the dynamics. More, precisely, below κ incidences are discovered as they tend to cluster around the shores and the mismatch between the line and the earthquake-like behavior in Fig. 1 denotes the potential number of missed drownings.

Data Availability Statement This manuscript has associated data in a data repository. [Authors' comment: The data used in the paper are available for download at the following link: https://mailaub-my.sharepoint.com/:x/g/personal/sn62_aub_edu_lb/ESVIF_Zdw3RON5ypLKypk00BkdpjBL3X8rOanTB0rAZUMg?e=K PsnOV].

References

1. R. Dendy, P. Helander, M. Tagger, Self-organised criticality in astrophysical accretion systems. *Phys. Scripta* **1999**(T82), 133 (1999)
2. P. Bak, C. Tang, Earthquakes as a self-organized critical phenomenon. *J. Geophys. Res. Solid Earth* **94**(B11), 15635–15637 (1989)
3. J. Davidsen, G. Kwiatek, Earthquake interevent time distribution for induced micro-, nano-, and pico-seismicity. *Phys. Rev. Lett.* **110**(6) (2013)
4. A. Corral, Long-term clustering, scaling, and universality in the temporal occurrence of earthquakes. *Phys. Rev. Lett.* **92**(10) (2004)
5. M.C. Stefanini, Spatio-temporal analysis of a complex landslide in the northern apennines (italy) by means of dendrochronology. *Geomorphology* **63**(3–4), 191–202 (2004)
6. J.A. Backer, J. Wallinga, Spatiotemporal analysis of the, ebola epidemic in west africa. *PLoS Comput. Biol.* **12**(12), 2016 (2014)
7. Q. Huang, L. Hu, Q.-B. Liao, J. Xia, Q.-R. Wang, H.-J. Peng, Spatiotemporal analysis of the malaria epidemic in mainland china, 2004–2014. *The Am. J. Trop. Med. Hyg.* **97**(2), 504–513 (2017)
8. B.D. Malamud, G. Morein, D.L. Turcotte, Forest fires: an example of self-organized critical behavior. *Science* **281**(5384), 1840–1842 (1998)
9. H. Stanley, L. Amaral, S.V. Buldyrev, P. Gopikrishnan, V. Plerou, M. Salinger, Self-organized complexity in economics and finance. *Proc. Nat. Acad. Sci.* **99**(suppl 1), 2561–2565 (2002)
10. R.J. Wijngaarden, M.S. Welling, C.M. Aegerter, M. Menghini, Avalanches and self-organized criticality in superconductors. *The Eur. Phys. J. B-Condens. Matter Complex Syst.* **50**(1–2), 117–122 (2006)
11. J. Hesse, T. Gross, Self-organized criticality as a fundamental property of neural systems. *Front. Syst. Neurosci.* **8**, 166 (2014)
12. D.R. Chialvo, Emergent complex neural dynamics. *Nat. Phys.* **6**(10), 744–750 (2010)
13. C. Bedard, H. Kroeger, A. Destexhe, Does the $1/f$ frequency scaling of brain signals reflect self-organized critical states?. *Phys. Rev. Lett.* **97**(11) (2006)
14. H.J. Jensen, *Self-Organized Criticality: Emergent Complex Behavior in Physical and Biological Systems*, vol. 10 (Cambridge University Press, 1998)
15. A.L. Goldberger, L.A. Amaral, J.M. Hausdorff, P.C. Ivanov, C.-K. Peng, H.E. Stanley, Fractal dynamics in physiology: alterations with disease and aging. *Proc. Natl. Acad. Sci.* **99**(suppl 1), 2466–2472 (2002)
16. D.L. Turcotte, *Fractals and Chaos in Geology and Geophysics* (Cambridge University Press, 1997)
17. E.-J. Wagenmakers, S. Farrell, R. Ratcliff, Human cognition and a pile of sand: a discussion on serial correlations and self-organized criticality. *J. Exp. Psychol. Gen.* **134**(1), 108 (2005)
18. R. Ramos, R. Sassi, J. Piqueira, Self-organized criticality and the predictability of human behavior. *New Ideas Psychol.* **29**(1), 38–48 (2011)
19. T. Kron, T. Grund, Society as a self-organized critical system. *Cybern. Human Know.* **16**(1–2), 65–82 (2009)
20. S. Galam, Sociophysics: a review of galam models. *Int. J. Mod. Phys. C* **19**(03), 409–440 (2008)
21. J. Davidsen, M. Paczuski, Analysis of the spatial distribution between successive earthquakes. *Phys. Rev. Lett.* **94**(4) (2005)
22. S. Najem, G. Faour, Debye-hückel theory for refugees’ migration. *EPJ Data Sci.* **7**(1), 1–9 (2018)
23. J.H. Ratcliffe, Aoristic signatures and the spatio-temporal analysis of high volume crime patterns. *J. Quant. Criminol.* **18**(1), 23–43 (2002)
24. L. Alessandretti, P. Sapiezynski, S. Lehmann, and A. Baronchelli, “Multi-scale spatio-temporal analysis of human mobility,” *PLoS one*, vol. 12, no. 2, 2017
25. T. U. M. A. International Organization for Migration, “The central mediterranean route: Migrant fatalities january 2014 - july 2017.”
26. M. Biggs, Strikes as forest fires: Chicago and paris in the late nineteenth century. *Am. J. Sociol.* **110**(6), 1684–1714 (2005)
27. H. Watt, M. Rice-Oxley, and D. Taylor, “Drowned, restrained, shot: how these migrants died for a better life,” Jun 2018
28. L. Tondo, “Italian coastguard finds bodies of migrants who drowned at sea,” Oct 2019
29. “Watch the med.”
30. R. Bullock, “Great circle distances and bearings between two locations,” *MDT*, June, vol. 5, 2007
31. G.M. Viswanathan, *The Physics of Foraging: An Introduction to Random Searches and Biological Encounters* (Cambridge University Press, 2011)